AGU PUBLICATIONS

JGR

Journal of Geophysical Research: Oceans

RESEARCH ARTICLE

10.1002/2013JC009152

Topographic scattering of the low-mode internal tide in the deep ocean

Manikandan Mathur[1], Glenn S. Carter[2], and Thomas Peacock[3]

[1]Department of Aerospace Engineering, Indian Institute of Technology Madras, Chennai, India, [2]Department of Oceanography, University of Hawaii at Manoa, Honolulu, Hawaii, USA, [3]Department of Mechanical Engineering, Massachusetts Institute of Technology, Cambridge, Massachusetts, USA

Key Points:
- Quantitative estimates of internal tide scattering by deep-ocean topography
- The analytical Green function method is validated by numerical simulations
- Tall topographic features play a dominant role in internal tide scattering

Correspondence to:
M. Mathur,
manims@ae.iitm.ac.in

Citation:
Mathur, M., G. S. Carter, and T. Peacock (2014), Topographic scattering of the low-mode internal tide in the deep ocean, *J. Geophys. Res. Oceans*, *119*, 2165–2182, doi:10.1002/2013JC009152.

Received 29 MAY 2013
Accepted 6 MAR 2014
Accepted article online 11 MAR 2014
Published online 3 APR 2014

Abstract We investigate the role of deep-ocean topography in scattering energy from the large spatial scales of the low-mode internal tide to the smaller spatial scales of higher modes. The complete Green function method, which is not subject to the restrictions of the WKB approximation, is used for the first time to study the two-dimensional scattering of a mode-1 internal tide incident on subcritical and supercritical topography of any form in arbitrary stratifications. For an isolated Gaussian ridge in a uniform stratification, large amplitude critical topography is the most efficient at mode-1 scattering and small amplitude topography scatters with an efficiency on the order of 5–10%. In a nonuniform stratification with a pycnocline, the results are qualitatively the same as for a constant stratification, albeit with the key features shifted to larger height ratios. Having validated these results by direct comparison with the results of nonlinear numerical simulations, and in the process demonstrated that WKB results are not appropriate for reasonable ocean predictions, we proceed to use the Green function approach to quantify the role of topographic scattering for the region of the Pacific Ocean surrounding the Hawaiian Islands chain. To the south, the Line Islands ridge is found to scatter ∼40% of a mode-1 internal tide coming from the Hawaiian Ridge. To the north, realistic, small-amplitude, rough topography scatters ∼5–10% of the energy out of mode 1 for transects of length 1000–3000 km. A significant finding is that compared to large extents of small-amplitude, rough topography a single large topographic feature along the path of a mode-1 internal tide plays the dominant role in scattering the internal tide.

1. Introduction

Internal waves play key roles in a myriad of large-scale and small-scale processes in the ocean. For example, it is now recognized that internal waves are an important consideration for the global-scale ocean energy budget as they represent a significant source of dissipation for barotropic tides and winds, the two primary sources of mechanical energy that drive ocean interior mixing [*Munk and Wunsch*, 1998]. An outstanding issue in physical oceanography, however, is determining the fate of this internal wave energy as it propagates through the ocean interior.

A global study of tidal energy dissipation, compiled using satellite altimetry data, revealed that approximately 1 TW of the total tidal dissipation occurs in the deep ocean, near areas of rough topography [*Egbert and Ray*, 2000]. Following this observation, internal tide generation at topographic features in the deep ocean has been actively investigated through field observations [e.g., *Rudnick et al*., 2003], analytical modeling [e.g., *Pétrélis et al*., 2006; *Echeverri and Peacock*, 2010], numerical modeling [e.g., *Carter et al*., 2008], and laboratory experiments [e.g., *Echeverri et al*., 2009]; a review is given by *Garrett and Kunze* [2007]. As such, it is now reasonable to say that internal tide generation in the ocean, at least in the prevalent linear and nominally two-dimensional regimes, is well understood.

One of the key outcomes from internal tide generation studies is a widespread belief that internal tide energy radiated in the form of short-wavelength vertical modes (i.e., $n > 2$, where n is the mode number) is dissipated in the vicinity of generation sites [*Garrett and Kunze*, 2007]. The processes believed to be involved in this dissipation are buoyancy-driven and shear-driven instabilities [*St. Laurent and Garrett*, 2002], which may or may not be coupled to scattering of internal wave beams by a nonuniform background stratification [*Mathur and Peacock*, 2009], energy conversion to solitary waves that propagate along the thermocline [*New and Pingree*, 1992; *New and Da Silva*, 2002], and interaction with background shear and turbulence

[*Staquet and Sommeria*, 2002]. The energy radiated in the long-wavelength vertical modes (i.e., $n = 1$ and 2), which is a majority of the energy radiated by significant topographic features, however, appears to travel far from the generation site. For example, *Ray and Mitchum* [1997] used satellite altimetry data to estimate that 15 GW of low-mode internal tide energy propagates over a thousand kilometers away from the Hawaiian Ridge; recent multisatellite altimetry studies by *Zhao et al*. [2012] further support this and estimate the semidiurnal internal wave fluxes to be even larger than those predicted by the analysis of data from a single satellite altimeter [*Ray and Mitchum*, 1997; *Ray and Cartwright*, 2001]. Thus, a key question is: where, and by what means, does this low-mode internal tide energy dissipate?

Possible dissipation mechanisms for the far-propagating low-mode internal tide include: wave-wave interactions such as the parametric subharmonic instability [e.g., *Staquet and Sommeria*, 2002; *MacKinnon and Winters*, 2005; *Tsang et al*., 2008], interactions with mean flows [e.g., *St. Laurent and Garrett*, 2002] and mesoscale structures [e.g., *Rainville and Pinkel*, 2006], and scattering by deep-ocean topography [e.g., *Johnston and Merrifield*, 2003] and continental shelves [e.g., *Kunze and Llewellyn Smith*, 2004]. At present, however, it is not clear what the relative importance of each mechanism is. Taking a step toward resolving this issue, we herein pursue some novel studies of deep-ocean topographic scattering.

The organization of the paper is as follows. In section 2, we review previous studies of internal tide scattering. The analytical Green function method is described in section 3, followed by a description of a supporting numerical model in section 4. In sections 5 and 6, we consider isolated Gaussian topographies in uniform and nonuniform stratifications, respectively. Two scenarios of realistic topography in realistic stratifications, these case studies being scattering by the Line Islands ridge and small-scale rough topography south and north of Hawaii, are then presented in section 7, followed by our conclusions in section 8.

2. Internal Tide Scattering in the Deep Ocean

Satellite observations, mainly from the waters surrounding Hawaii, suggest significant scattering of internal wave energy occurs at tall topography, and only weak scattering over small-scale rough topography. For example, at the Line Islands Ridge there is a rapid decay of the large, southwest propagating mode-1 baroclinic energy flux generated at French Frigate Shoals [*Ray and Cartwright*, 2001], coinciding with an abrupt change in wave number and amplitude of the internal tide surface elevations [*Ray and Mitchum*, 1997; *Johnston et al*., 2003]. Heading north from the Hawaiian ridge system, however, *Zhao et al*. [2012] show that low-mode internal tides propagate over 3500 km across the generally small-scale, rough topography of the North Pacific Ocean.

There have been several analytical studies of internal tide scattering by ocean floor topography, but debate still remains about whether this process is efficient at transferring energy from low to high modes. Early studies of low-mode internal-tide scattering by isolated topography in a finite-depth ocean were performed by *Larsen* [1969], and *Robinson* [1969], who considered a two-dimensional, knife edge barrier. In both cases, the governing wave equation was assumed to be linear and inviscid, and this was also the case for all subsequent theoretical studies of internal wave scattering by topography. As detailed in section 3, it is the Green function approach used by *Robinson* [1969] that we revisit in this paper, albeit with the substantial improvement of removing the restrictions of idealized two-dimensional topography and uniform stratification.

A number of theoretical studies have considered scattering by subcritical (i.e., topographic slope less than internal ray slope), infinitesimal topography using perturbation methods [e.g., *Cox and Sandstrom*, 1962; *Rubenstein*, 1988; *Müller and Xu*, 1992]. An advantage of this approach is that the ocean floor boundary condition (implemented on a flat bottom) can be Fourier decomposed and predictions made for three-dimensional topography. For typical internal wave and bottom topography spectra in the ocean, some of these studies estimated that 6–10% of the incident low-mode energy flux is redistributed by scattering; *Rubenstein* [1988] actually predicted notably stronger scattering but via seemingly incorrect reasoning [*Müller and Xu*, 1992]. This modest estimate was supported by *St. Laurent and Garrett* [2002], who determined a $\sim$10% conversion rate using a so-called second generation scattering calculation for infinitesimal topography; this approach took the characteristic velocity near the ocean floor due to a mode-1 internal tide and estimated the generation of internal waves by rough topography as a proxy for scattering. *Müller and Xu* [1992] noted, however, that calculations based on infinitesimal topography are only marginally valid for typical ocean conditions and that scattering becomes more efficient for larger and more rugged

topography; estimates based on infinitesimal topography may therefore only represent a lower bound for the ocean.

There have been few theoretical studies of scattering by finite-amplitude topography. *Gilbert and Garrett* [1989] focused on the importance of critical points (i.e., where the topographic slope equals the internal ray slope) and concluded that locally convex topography is more efficient at scattering than locally concave topography; this model assumed an infinitely deep ocean. *Müller and Liu* [2000a] used a mapping function based on ray tracing to investigate scattering by several different forms of finite-amplitude topography. They found that the efficiency of scattering by finite-amplitude topography is more substantial than for infinitesimal topography and, broadly speaking, that subcritical and supercritical (i.e., topographic slope greater than internal ray slope) ridges transmit and reflect internal wave energy, respectively. The authors applied their approach to a random superposition of plane waves with a Garret-Munk spectrum [*Müller and Liu*, 2000b], and although no general quantitative results for scattering efficiency were stated it was concluded that scattering at finite-amplitude topography causes significant distortion to the incident spectrum.

Most recently, *Bühler and Holmes-Cerfon* [2011] advanced the approach of *Müller and Liu* [2000a] to build a numerical tool with which they studied the decay of a mode-1 internal tide due to interactions with finite-amplitude, subcritical seafloor topography over a substantial length of propagation in a uniformly stratified ocean. Their results suggest that scattering by finite-amplitude random topography can provide a rapid decay mechanism for low-mode internal tides. Based on statistical calculations for many realizations of random topography, the method predicts an exponential decay rate that scales quadratically and inversely with the height and correlation length scale of the topography, respectively. Significantly, for realistic ocean values, this suggests an *e*-folding decay scale for the low-mode internal tide in the range 250–500 km, implying that deep-ocean scattering is indeed an important decay process.

While the studies of *Müller and Liu* [2000a, 2000b] and *Bühler and Holmes-Cerfon* [2011] provide significant insight, these approaches are based on several idealizations. The first is two-dimensionality, which is a reasonable first approximation for many slopes and ridges, although clearly not for seamounts [*Müller and Liu*, 2000b]; we are also beholdent to this two-dimensionality approximation for the Green function analysis in this paper. Furthermore, *Müller and Liu* [2000a, 2000b] and *Bühler and Holmes-Cerfon* [2011] considered an ocean with uniform stratification, with the latter authors also being restricted to subcritical topography.

Detailed numerical studies of the scattering of a mode-1 internal tide by finite-amplitude Gaussian topography were performed by *Johnston and Merrifield* [2003]. A conclusion of their study was that, in general, the height of the topography affects the extent of energy transmission and reflection, while the slope and the width of the topography determine how much energy gets scattered into higher modes, which is somewhat different from the conclusions of *Müller and Liu* [2000a]. Subsequently, *Johnston et al*. [2003] studied the scattering of a mode-1 internal tide, generated at the Hawaiian ridge, by the Line Islands ridge, where the height ratio (i.e., the ratio of the topographic height relative to the total water depth) can exceed 0.5. Around 19% of the incident energy was found to be scattered into modes 2–5, and a further 18% was lost to a combination of dissipation by the numerical turbulence parameterization and nonlinear energy transfer to higher harmonics. It was concluded that scattering by seafloor topography could be a significant process in the Western Pacific. *Legg* [2014] recently performed a numerical study of finite-amplitude low-mode internal waves incident on isolated topography and found that energy dissipation at subcritical slopes increases as a function of the height of the topography and the incident wave amplitude. Performing a couple of simulations for 3-D axisymmetric topographies, *Legg* [2014] also made the important observation that internal tide scattering by 3-D topographies is more suited for 2-D modeling than internal tide generation at 3-D topographies.

In support of the effort to clarify the importance of deep-ocean topographic scattering, in this paper, we exploit recent advances in the Green function approach to investigate the efficiency of this process. Since this method can handle arbitrary two-dimensional topography and stratifications it allows us to remove many of the idealizations that were present in previous models and investigate scenarios that are increasingly relevant to the ocean. In so doing, we identify a key aspect of topographic scattering that has been overlooked: that the impact of a single tall ridge somewhere along the path traveled by a low-mode internal tide can far exceed the cumulative impact of small-scale topography.

3. Theory

We define a stream function $\psi(x,z,t)$ so that the associated internal tidal velocities are $(u,w)=(-\psi_z,\psi_x)$, x and z being the horizontal and vertical coordinates, respectively, and t being time. The stream function of the total wavefield is $\psi(x,z,t)=\psi_b(x,z,t)+\psi'(x,z,t)$, where ψ_b represents the background internal tide and ψ' is the perturbation to ψ_b due to scattering by topography. It is assumed that the response is at the same frequency, ω, as the background internal tide, i.e., $\psi_b(x,z,t)=\Re[\phi_b(x,z)e^{-i\omega t}]$ and $\psi'(x,z,t)=\Re[\phi'(x,z)e^{-i\omega t}]$, where ϕ_b and ϕ' are complex amplitudes, with $\Re$ denoting the real part. The velocity component along the second horizontal direction y is given by $v=\Re[(if/\omega)(\phi_{b,z}+\phi'_z)e^{-i\omega t}]$, where the Coriolis frequency $f=2\Omega_n=2\Omega\sin\theta_{lat}$ is twice the background rotation Ω_n. Ω and θ_{lat} are the earth's background rotation and latitude of the region of interest, respectively.

The Green function approach, a theoretical framework in the limit of linear, inviscid, and Boussinesq approximations for modeling the interaction of internal waves with topography, expresses the perturbation wavefield, ϕ' as an integral over contributions from a distribution of sources of strength $\gamma(x')$ placed on the topography $(x',z')=(x',h(x'))$ [*Robinson*, 1969; *Pétrélis et al*., 2006; *Balmforth and Peacock*, 2009; *Echeverri and Peacock*, 2010], i.e.,

$$\phi'(x,z)=\int_{-a}^{b}\gamma(x')G(x,x';z,h(x'))dx', \tag{1}$$

where $[-a,b]$ are the horizontal limits of the topography and $G(x,x';z,z')$ is the Green function. The continuous function $h(x)$ is assumed to be in the range $0\le h(x)<H$ for $x\in[a,b]$, going smoothly to zero at $x=-a$ and $x=b$. Outside the $x\in[a,b]$ domain, $h(x)$ is assumed to be uniformly zero.

The Green function can be expressed as a sum over the vertical modes of the stratification, Φ_n, via the relation:

$$G(x,x';z,z')=\sum_{n=1}^{n=\infty}\frac{\Phi_n(z')}{2k_n}\left(\int_0^H\frac{N(z)^2-\omega^2}{\omega^2-f^2}\Phi_n^2dz\right)^{-1}e^{ik_n|x-x'|}\Phi_n(z), \tag{2}$$

where the nth mode satisfies

$$\Phi_{n,zz}+\frac{N(z)^2-\omega^2}{\omega^2-f^2}k_n^2\Phi_n=0, \tag{3}$$

with homogeneous boundary conditions $\Phi_n(0)=\Phi_n(H)=0$ at the ocean floor ($z=0$) and free surface ($z=H$), and the positive eigenvalue k_n is the corresponding horizontal wave number [*Robinson*, 1969; *Pétrélis et al*., 2006; *Echeverri and Peacock*, 2010]. Equation (3), with the homogeneous boundary conditions, constitutes a Sturm-Liouville system that must be solved numerically to obtain Φ_n for an arbitrary stratification $N(z)$. For convenience, and without any loss of generality, we define Φ_n such that $|d\Phi_n/dz|$ has a maximum value of unity for $z\in[0,H]$.

In the limit of a uniform stratification (i.e., $N(z)=N_0$), the vertical modes $\Phi_n(z)=(H/n\pi)\sin(n\pi z/H)$ and the eigenvalues $k_n=n\pi/(H\cot\theta)$, where $\cot\theta=\sqrt{(N_0^2-\omega^2)/(\omega^2-f^2)}$. This idealized scenario has been studied in the contexts of scattering [*Robinson*, 1969] and generation [e.g., *Pétrélis et al*., 2006]. Wentzel-Kramers-Brillouin (WKB) versions of the vertical modes have been used to represent the Green function for studies of generation [e.g., *Llewellyn Smith and Young*, 2002, 2003; *Echeverri and Peacock*, 2010]. Here we use the complete Green function for an arbitrary background stratification $N(z)$, in which case combining equation (1) with the full Green function (2) gives the expression for the perturbation stream function:

$$\phi'(x,z)=\sum_{n=1}^{n=\infty}\left(\int_0^H\frac{N(z)^2-\omega^2}{\omega^2-f^2}\Phi_n^2dz\right)^{-1}\frac{\Phi_n(z)}{2k_n}\int_{-a}^{b}\gamma(x')\Phi_n(h(x'))e^{ik_n|x-x'|}dx', \tag{4}$$

with H being the far-field ocean depth.

No normal-flow at the ocean-floor topography $h(x)$ and the sea surface (approximated as a rigid lid) require:

$$\phi'(x,h(x)) = -\phi_b(x,h(x)) + \phi_b(x,0) \quad \text{and} \quad \phi'(x,H) = 0, \tag{5}$$

where the functional form of ϕ_b, which is assumed to satisfy the no normal-flow boundary condition at $z = 0$ and $z = H$, depends on the background internal tide. Throughout this paper, we focus on an incident mode-1 internal tide propagating from left to right, in which case:

$$\phi_b(x,z) = -\Phi_1(z)e^{ik_1 x}. \tag{6}$$

For comparison, studies of internal tide generation by barotropic forcing, a scenario for which the WKB Green function approach been extensively applied [*Echeverri and Peacock*, 2010], use $\phi_b(x,z) = -Uz$ in the boundary condition, where U is the barotropic forcing velocity.

Substituting (6) into the lower boundary condition in (5) and using the Green function solution (4) results in the integral equation:

$$\Phi_1(h(x))e^{ik_1 x} = \sum_{n=1}^{n=\infty} \left(\int_0^H \frac{N(z)^2 - \omega^2}{\omega^2 - f^2} \Phi_n^2 dz \right)^{-1} \frac{\Phi_n(h(x))}{2k_n} \int_{-a}^{b} \gamma(x')\Phi_n(h(x'))e^{ik_n|x-x'|} dx', \tag{7}$$

which is solved numerically for $\gamma(x)$ using the procedure detailed in *Echeverri and Peacock* [2010]. In solving this numerically, one must use a sufficiently fine spatial resolution to represent the topography and a sufficiently large number of modes in the summation so that the solution converges. We note here that replacing the mode shapes $\Phi_n(z)$ and the horizontal wave number k_n by the WKB mode shapes and corresponding horizontal wave numbers constitutes the Green function theory with the WKB approximation [*Llewellyn Smith and Young*, 2003; *Echeverri and Peacock*, 2010], referred to as the WKB theory in the rest of this paper.

In the far field, where the ocean depth is constant, one can define

$$a_n^{\pm} = \frac{1}{2k_n} \left(\int_0^H \frac{N(z)^2 - \omega^2}{\omega^2 - f^2} \Phi_n^2 dz \right)^{-1} \int_{-a}^{b} \gamma(x')\Phi_n(h(x'))e^{\mp ik_n x'} dx', \tag{8}$$

where a_n^+ corresponds to $x > b$ and a_n^- to $x < -a$. The perturbation stream function can thus be written explicitly and concisely as a sum over the vertical modes:

$$\phi'(x,z) = \sum_{n=1}^{n=\infty} a_n^{\pm} \Phi_n(z) e^{\pm ik_n x}. \tag{9}$$

The total wavefield is $\phi(x,z) = \phi_b + \phi'$ with ϕ_b being given by the expression in (6). With the exception of transmitted mode 1, the transmitted (T) and reflected (R) depth-averaged energy flux in mode-n normalized by the incident energy flux in mode 1 is:

$$C_n^{T,R} = |a_n^{\pm}|^2 \frac{k_1}{k_n} \frac{\int_0^H (d\Phi_n/dz)^2 dz}{\int_0^H (d\Phi_1/dz)^2 dz}. \tag{10}$$

For the energy flux in the transmitted mode 1, one must include the contribution from ϕ_b, in which case:

$$C_1^T = |-1 + a_1^+|^2. \tag{11}$$

For future discussion, it is also convenient to define the cumulative transmitted and reflected energy fluxes in mode-p through mode-q:

$$C_{p-q}^{T+R}=\sum_{n=p}^{n=q}(C_n^T+C_n^R). \quad (12)$$

4. Methods

In this section, we summarize details of the parameters used for numerically solving the integral equation (7) and present an overview of the numerical model used to validate and complement the predictions from the Green function theory.

4.1. Analysis

In principle, equations (7) and (9) require $n=\infty$ to completely represent the solution, but in practice the sum is truncated at a finite value of n above which the solution changes negligibly. Furthermore, in solving (7) both the x and z spatial coordinates must be discretized, again seeking to achieve numerical convergence of the solution. To achieve convergence, we increased the spatial and then modal resolutions until the energy conservation equation $C_{1-n}^{T+R}=1$ was satisfied with an error of $<1\%$, unless specified otherwise. Typically, $n=500$ and $n=200$ were used for uniform and nonuniform stratifications, respectively, and the topography was discretized by 2500 points, though these values varied somewhat depending on the specific case being solved. The number of modes used to calculate the wavefields and energy transmission/reflection coefficients was usually smaller than the value of n used to compute the distribution $\gamma(x)$. Finally, since nondimensionalizations such as those employed in *Echeverri and Peacock* [2010] become quite cumbersome when considering a fully nonuniform stratification, we instead used reasonable dimensional parameters that are representative of the ocean. Unless stated otherwise, $H=3800$ m, $\omega=1.4053\times10^{-4}$ rad/s (M2), and $N^2=3\times10^{-5}$ rad/s were used as the basis for our idealized studies; for simplicity we set $f=0$ for the idealized studies and utilized physical values of f for our ocean case studies. We also note here that the case of a uniform stratification satisfies the relation $k_n=nk_1$, resulting in a spatially coherent wave beam pattern of the scattered wavefield; the nonuniform stratification does not admit the relation $k_n=nk_1$, thus resulting in a spatially less coherent scattered wavefield.

4.2. Numerics

To rigorously test the complete Green function approach, which has never been used to study scattering for arbitrary topography in uniform and nonuniform stratifications, we ran a number of corresponding numerical simulations using a modified version of the nonlinear, hydrostatic, terrain following (sigma coordinate) Princeton Ocean Model [*Blumberg and Mellor*, 1987]. A mode-1 internal tide was propagated down a narrow channel, which consisted of the topography of interest extended in both directions using a constant depth. To best match the analytical results, the simulations used a rigid lid at the surface (i.e., the baroclinic modes have no surface expression), and zero dissipation was applied to momentum and buoyancy. At the far end of the channel the relaxation boundary condition of *Carter and Merrifield* [2007] prevented energy in all modes from being reflected. Modal decomposition of the model output was performed over the flat bottom sections upstream and downstream of the topographic feature. The number of grid points in the vertical direction used by the numerical simulations were 54, 150, 200, and 224 for the cases in sections 5, 6, 7.1, and 7.2, respectively; assuming at least five points per wavelength, the highest mode that the numerical simulations resolved was 25, 18, 17, and 18, respectively. For the nonuniform stratifications considered in sections 6 and 7, the zero crossings of the modes are crowded near the ocean surface, requiring a larger number of points to accurately resolve a given mode number than for a uniform stratification.

5. Uniform Stratification

We first consider the scattering of a mode-1 tide by an isolated Gaussian ridge in an ocean with uniform stratification. This allows several fundamental investigations of internal tide scattering, as well as initial confirmation of the accuracy and reliability of the Green function method.

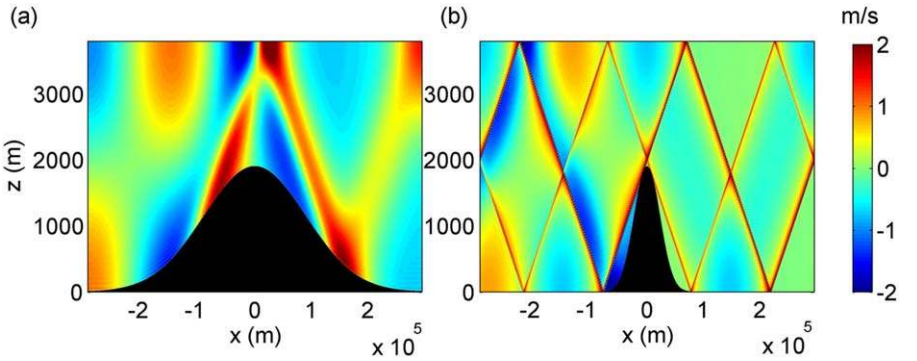

Figure 1. The horizontal velocity field $u(x,z,t)$ at an arbitrary instant in time for mode-1 (incident from the left) scattering by a (a) subcritical ($\epsilon = 0.5$) and (b) supercritical ($\epsilon = 2$) Gaussian ridge of height ratio $h^* = 0.5$ in a uniform stratification (calculated using the Green function model).

For the isolated Gaussian ridge

$$h_G(x) = h_0 e^{-x^2/2\sigma^2}, \tag{13}$$

we define the criticality to be $\epsilon = \max(dh_G/dx)/\tan\theta$, this being the ratio of the maximum topographic slope to the internal ray slope, and the height ratio to be $h^* = h_0/H$; for a uniform stratification, these two dimensionless parameters completely characterize the system. Figures 1a and 1b show the horizontal velocity $u(x,z,t)$ at an arbitrary phase in the subcritical ($\epsilon = 0.5$) and supercritical ($\epsilon = 2$) regimes, respectively, for $h^* = 0.5$. The results presented in this figure, and indeed in all uniform stratification results, use only the first 100 modes to represent the solution (although more modes, up to 500, were available from the calculation of the quantity γ that underlies the solution). For the subcritical scenario, the mode-1 internal tide that is incident from the left passes relatively unscathed, while scattering is apparent for the supercritical scenario, giving rise to transmitted and reflected wavefields with beam-like features due to the presence of high modes.

Figures 2a and 2b present the variation of the transmitted (C^T_{1-100}) and reflected (C^R_{1-100}) energy fluxes, respectively, with criticality and height ratio. The results for $\epsilon < 0.9$ reveal essentially complete transmission of energy and, accordingly, no significant reflection of energy in the subcritical regime for all depth ratios. The system exhibits a sharp decrease in C^T_{1-100}, and thus increase in C^R_{1-100}, near criticality ($\epsilon = 1$), the rapidity of the change being more pronounced for larger height ratios. For supercritical regimes with $\epsilon > 3$, the variation of transmission and reflection with depth ratio becomes essentially independent of criticality, and the supercritical ridge effectively behaves as a knife edge; we verified this by confirming that in the limit $\epsilon \to \infty$ our results agree with the knife-edge results for $h^* = 0.75$ presented in Figure 3 of *Müller and Liu* [2000a]. For small height ratios ($h^* < 0.2$), the transmission and reflection coefficients are essentially independent of criticality, with the vast majority of the energy being transmitted and little reflected.

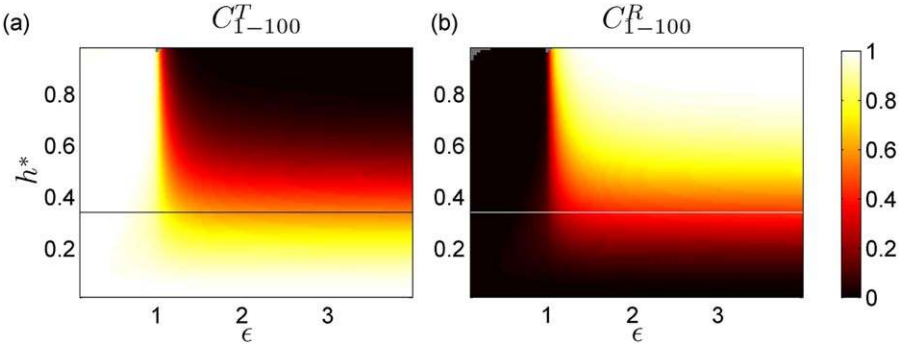

Figure 2. The fraction of the incident energy flux scattered into the (a) transmitted and (b) reflected wavefields as a function of ϵ and h^* for isolated Gaussian topography in a uniform stratification (calculated using the Green function model). The black and white horizontal lines in Figures 2a and 2b, respectively, correspond to $h^* = 0.34$.

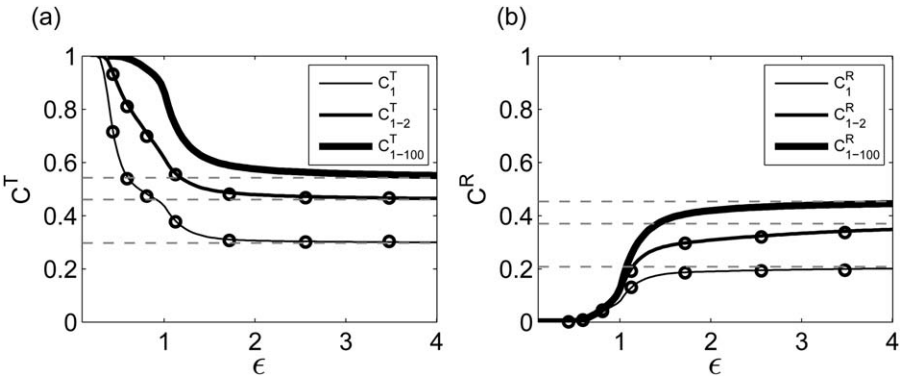

Figure 3. The fraction of the incident energy flux scattered into the (a) transmitted and (b) reflected wavefields as a function of ϵ for $h^* = 0.34$ in a uniform stratification. The three solid curves in each plot correspond to the cumulative energy flux up to modes 1, 2, and 100, calculated using the Green function model. Numerical results for $\epsilon = 0.43, 0.59, 0.81, 1.13, 1.72, 2.56$, and 3.48 are shown by the circles (◦). The horizontal dashed lines indicate the corresponding values for a knife-edge topography of the same height ratio ($h^* = 0.34$), calculated using the Green function model with $\epsilon = 20$.

Having established the functional dependence of transmitted and reflected energy flux, the next step is to consider the transfer of energy flux from lower to higher modes. To investigate this aspect of the scattering process, for $h^* = 0.34$ (indicated by the horizontal black and white lines in Figures 2a and 2b, respectively) the variations with criticality of C_1^T, C_{1-2}^T, and C_{1-100}^T, these being the cumulative transmitted energy fluxes up to modes 1, 2, and 100, and correspondingly C_1^R, C_{1-2}^R, and C_{1-100}^R, are presented in Figures 3a and 3b, respectively. These results show that scattering from mode 1 to higher modes in the transmitted and reflected wavefields increases as criticality ($\epsilon = 1$) is transcended from below. To validate our analytical results, the results of seven complementary numerical simulations are also included in Figures 3a and 3b, and these show excellent agreement with the theoretical results. It was not possible to calculate C_{1-100}^T and C_{1-100}^R from the numerical data owing to strong numerical/viscous dissipation for the higher modes and a lack of vertical grid resolution to resolve the very high modes. For the cases studied by numerical simulations, our theory predicts that the maximum energy in the unresolved modes (>25) is 2.8% of the incident mode-1 energy.

While the results in Figures 2 and 3 set the scene, it is perhaps most important to quantify how much energy is scattered into higher modes in both the transmitted and reflected wavefields combined, as this represents the total energy transfer from larger to smaller spatial scales that are more prone to instability and dissipation. This motivated the calculation of the scattering efficiency $C_{2-\infty}^{T+R} = 1 - C_1^T - C_1^R$ (i.e., the total energy scattered into modes 2 through ∞ in both the transmitted and reflected wavefields) as a function of the criticality ϵ and the height ratio h^*. Figure 4 presents the variation of $C_{2-\infty}^{T+R}$ with criticality and height ratio. The key result is that the maximum efficiency of scattering to higher modes occurs around criticality, where there is a complex dependence of $C_{2-\infty}^{T+R}$ with both depth ratio and criticality for $h^* > 0.4$ and $0.8 < \epsilon < 1.2$. The existence of a series of local maxima in parameter space is a phenomenon reminiscent of resonant transmission of internal waves in nonuniform stratifications [*Sutherland and Yewchuk*, 2004; *Mathur and Peacock*, 2010]. For supercritical topography there is a relatively straightforward functional dependence of the scattering efficiency on depth ratio, having a maximum in the vicinity of $h^* = 0.4$ (for strongly supercritical, knife-edge topography the maximum value is

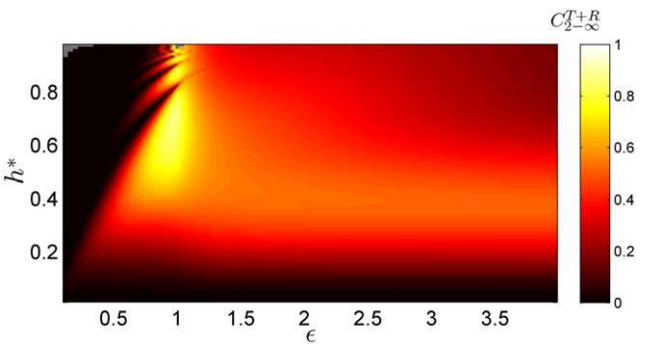

Figure 4. The fraction of the incident energy flux scattered into transmitted and reflected modes 2 through ∞, $C_{2-\infty}^{T+R} = 1 - C_1^T - C_1^R$, as a function of ϵ and h^* for an isolated Gaussian ridge in a uniform stratification (calculated using the Green function model).

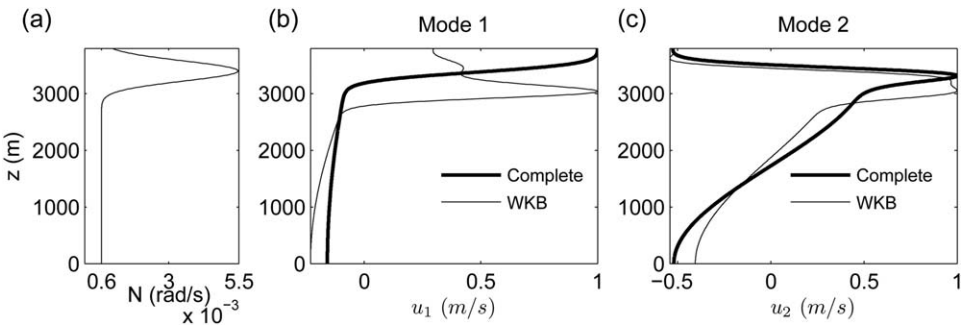

Figure 5. (a) A nonuniform stratification $N(z)$ representative of the ocean. The horizontal velocity $u(z)=d\Phi(z)/dz$ for (b) mode-1 and (c) mode-2 for the stratification in Figure 5a, as determined by numerically solving (3) (thick solid line) and using the WKB approximation (thin solid line). The stream functions are normalized so that $\max(|d\Phi_1/dz|)=\max(|d\Phi_2/dz|)=1\mathrm{m/s}$.

0.51 for $h^* = 0.37$). For small depth ratios ($h^* < 0.4$), the scattering efficiency increases monotonically, but weakly, with criticality.

There are two key conclusions to be drawn from these initial studies. The first conclusion is that for small height ratios ($0 < h^* < 0.2$), the scattering efficiency increases monotonically with h^* and ϵ. Thus, for small-scale topography on the ocean floor, the taller and steeper the ridge, the more significant its ability to scatter the mode-1 internal tide. The second conclusion is that for larger height ratios ($0.2 < h^* < 1.0$) scattering is most efficient near criticality. Additionally, the results show that criticality plays the primary role in determining whether the internal tide is transmitted or reflected. These results are consistent with the observations of *Müller and Liu* [2000a] that subcritical and supercritical topographies transmit and reflect the low-mode internal tide, respectively, and scattering to higher modes is significant for near-critical topography. This is somewhat different from the conclusion of *Johnston and Merrifield* [2003] that it is the height ratio that primarily affects energy transmission and reflection, while the slope and the width of the topography determine the conversion to higher modes. We note, however, that for a Gaussian ridge the slope and the width together specify the topographic shape completely, and hence the conclusion of *Johnston and Merrifield* [2003] does not isolate the effects of ϵ and h^*.

6. Nonuniform Stratification

We now proceed to study the scattering of a mode-1 tide by isolated topography in a nonuniform stratification that is characteristic of the ocean. This course of action is chosen because the primary interest is in assessing the importance of scattering for a typical ocean scenario and not to get embroiled in studies of an extensive, multidimensional parameter space due to the introduction of several more parameters (e.g., pycnocline strength, pycnocline location, and pycnocline length scale). Indeed, the uniform stratification results suggest that for small amplitude topography ($h^* < 0.1$) the exact location and width of the pycnocline in the upper ocean will have little impact on the scattering, whereas for large amplitude topography ($h^* > 0.5$) the system will be sensitive to the specifics of the upper ocean stratification and should be dealt with on a case-by-case basis.

The model stratification, presented in Figure 5a, comprises a uniform stratification with $N_0 = 6\times10^{-4}$ rad/s at large depths ($z \approx 0$) and a Gaussian pycnocline of characteristic width 500 m and maximum stratification 5.48×10^{-3} rad/s centered around $z = 3400$ m in an ocean of depth 3800 m. For simplicity, we refrain from including background rotation at this point (i.e., $f = 0$), saving it for our case studies in section 7. The shapes of modes 1 and 2 for the stratification in Figure 5a are presented in Figures 5b and 5c, respectively. It is evident that for this stratification the true (complete) modes 1 and 2 differ noticeably from their WKB counterparts, and thus it would seem prudent to use the complete Green function approach to study scattering in this stratification.

In a nonuniform stratification, the definition of criticality is complicated by the varying topographic slope and stratification. We define the criticality of the Gaussian ridge (13) to be $\epsilon = \max((dh_G/dx)/tan\theta)$, i.e., the maximum ratio of the topographic slope to the local internal wave ray slope. Figures 6a and 6b present the horizontal velocity $u(x,z,t)$ at an arbitrary instant in time for a mode-1 internal tide incident on a subcritical

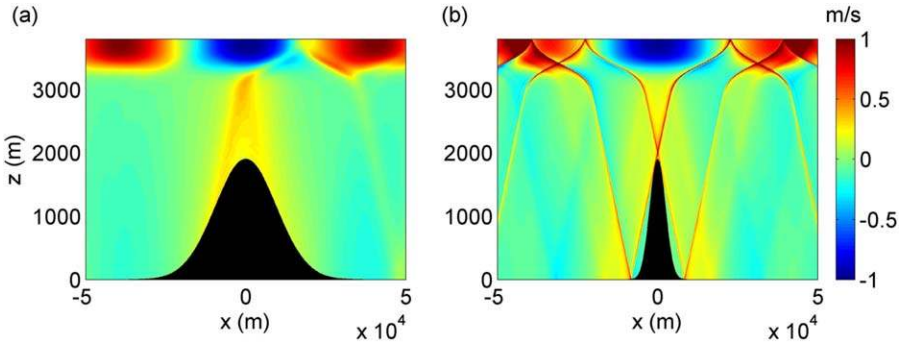

Figure 6. The horizontal velocity field $u(x,z,t)$ at an arbitrary instant in time for mode-1 (incident from the left) scattering in a nonuniform stratification by a (a) subcritical ($\epsilon = 0.5$) and (b) supercritical ($\epsilon = 2$) Gaussian ridge with h^*=0.5 (calculated using the Green function model).

($\epsilon = 0.5$) and supercritical ($\epsilon = 2$) ridge, respectively, for $h^* = 0.5$. The presentation of these wavefields, and all other nonuniform stratification results, was achieved using the first 50 of the 200 vertical modes used for the determination of $\gamma(x)$. For both scenarios, the incident mode-1 internal tide is transmitted with very little scattering to higher modes. This result is qualitatively different from that presented for ridges of the same height ratio in a uniform stratification in Figure 1, and is due to the dominant activity of the wavefield existing well above the ridge, in the pycnocline.

Setting $h^* = 0.85$, so that the Gaussian ridge penetrates the pycnocline, produces significant scattering to higher modes for both subcritical ($\epsilon = 0.5$) and supercritical ($\epsilon = 2$) scenarios, as is evident by the wavefields presented in Figures 7a and 7b. To investigate further, Figures 8a and 8b present the variation of the transmitted (C^T_{1-50}) and reflected (C^R_{1-50}) energy fluxes, respectively, with criticality and height ratio. The qualitative features closely resemble those for the uniform stratification scenario in Figure 2, albeit with the key features occurring for larger values of h^*.

Figures 9a and 9b present the variation with criticality of the transmitted and reflected energy fluxes for $h^* = 0.85$, alongside comparisons with numerical and WKB results. The nature of the results is reminiscent of those for uniform stratification and $h^* = 0.34$ in Figures 3a and 3b. There is substantial reflection as the criticality increases through unity, significant scattering out of mode 1 occurs for $\epsilon > 0.5$, and for $\epsilon > 2$ the ridge effectively behaves like a knife edge. The excellent agreement with numerical results (for the cases studied by numerical simulations, our theory predicts that the maximum energy in the unresolved modes (>18) is 2.6% of the incident mode-1 energy) confirms the accuracy of the complete Green function approach for nonuniform stratifications. In contrast, the WKB results differ significantly, revealing that the WKB approximation can provide misleading results. For example, at criticality the WKB method under predicts the transmitted mode-1 energy flux (0.34 instead of 0.47) while simultaneously over predicting the total transmitted energy flux (0.96 instead of 0.79).

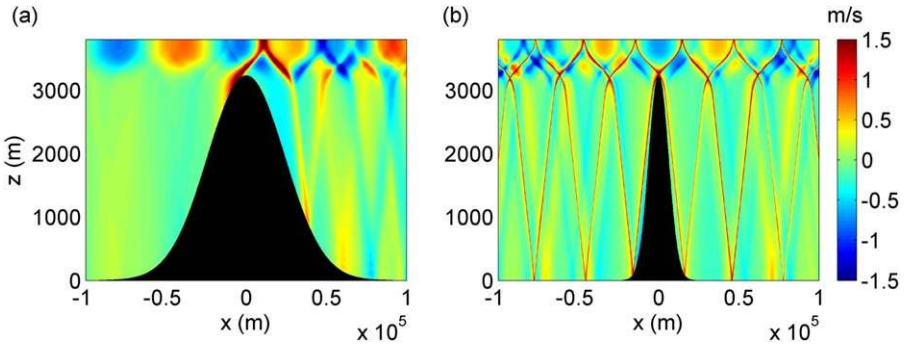

Figure 7. The horizontal velocity field $u(x,z,t)$ at an arbitrary instant in time for mode-1 (incident from the left) scattering in a nonuniform stratification by a (a) subcritical ($\epsilon = 0.5$) and (b) supercritical ($\epsilon = 2$) Gaussian ridge with h^*=0.85 (calculated using the Green function model).

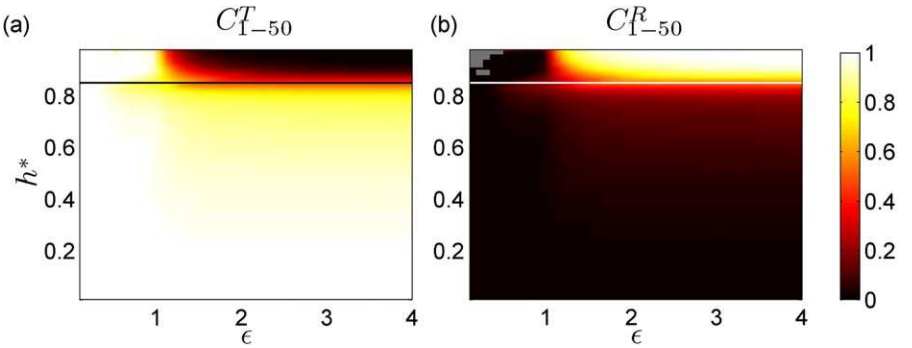

Figure 8. The fraction of the incident energy flux scattered into the (a) transmitted and (b) reflected wavefields as a function of ϵ and h^* for an isolated gaussian topography in the nonuniform stratification presented in Figure 5a (calculated using the Green function model). The black and white horizontal lines in Figures 8a and 8b, respectively, correspond to $h^* = 0.85$.

Plotting the scattering efficiency $C^{T+R}_{2-\infty}$ as a function of ϵ and h^*, in Figure 10a, reproduces results qualitatively similar to those presented in Figure 4 for a uniform stratification, with the key features shifted to larger values of h^*. For $h^* < 0.5$, $C^{T+R}_{2-\infty}$ is small for all criticalities. Scattering to higher modes becomes most efficient at criticality and there is a sequence of maxima and minima with increasing height ratio for near-critical topography, as h^* impinges upon and penetrates the pycnocline. In the strongly supercritical regime, i.e., for a knife-edge topography, the scattering efficiency attains a maximum of $C^{T+R}_{2-\infty}$=0.5 at $h^* = 0.85$; we recall that the maximum scattering efficiency for a knife-edge topography in a uniform stratification was found to be $C^{T+R}_{2-\infty}$=0.51 occurring at $h^* = 0.37$.

Figure 10b presents the difference in $C^{T+R}_{2-\infty}$ between the Green function models with and without the WKB approximation. Expressions for energy fluxes as a function of mode strengths within the WKB approximation have previously been discussed by *Echeverri and Peacock* [2010]; we note, however, that the expression for $C^{\pm}$ in equation (2.16) in *Echeverri and Peacock* [2010] has to be corrected by a multiplicative factor of $\omega^2/(\omega^2-f^2)$. Even for relatively small height ratios $(h^* \sim 0.3-0.5)$, for which the topography peak is well below the pycnocline, the WKB approximation results in a significant error ($\sim$0.25) in the scattering efficiency. This result is somewhat in contrast to a previous assertion that the WKB approach is not misleading even for mode 1 and modest amplitude topography [*Llewellyn Smith and Young*, 2002]. The discrepancy becomes particularly striking near criticality when the topography peak is in the vicinity of the pycnocline.

Overall, we conclude that the dependence of scattering on the height ratio and criticality in a nonuniform stratification typical of the ocean is qualitatively similar to scattering in a uniform stratification, with the exception that, as one might expect, the parameter space boundaries that delineate noticeable changes in behavior are shifted to greater height ratios due to the presence of a pycnocline. Thus, while large

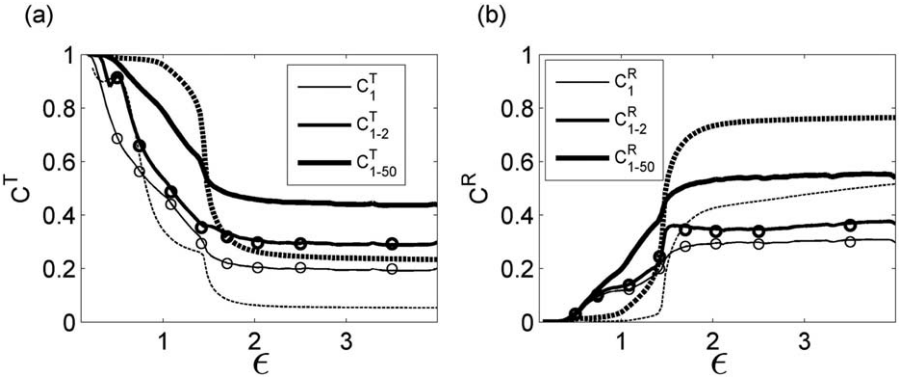

Figure 9. The fraction of the incident energy flux scattered into the (a) transmitted and (b) reflected wavefields as a function of ϵ for $h^* = 0.85$, for the nonuniform stratification shown in Figure 5a. The three solid curves in each plot correspond to the cumulative energy flux up to modes 1, 2, and 50, calculated using the Green function model. The dashed curves represent the WKB results for C^T_1, C^T_{1-50} and C^R_1, C^R_{1-50}. Numerical results for C^T_1, C^T_{1-2} and C^R_1, C^R_{1-2} are plotted as circles.

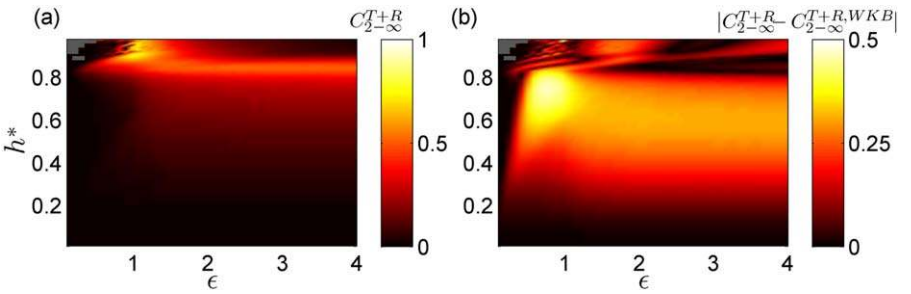

Figure 10. (a) The fraction of the incident energy flux scattered into transmitted and reflected modes 2 through ∞, $C_{2-\infty}^{T+R} = 1 - C_1^T - C_1^R$, as a function of ϵ and h^* for an isolated Gaussian topography in the nonuniform stratification shown in Figure 5a (calculated using the Green function model). (b) The absolute difference in $C_{2-\infty}^{T+R}$ between the Green function models with and without the WKB approximation.

amplitude topography can produce some nontrivial results, small amplitude isolated topography is responsible only for weak scattering with an efficiency on the order of 5–10% that increases monotonically with depth ratio and criticality.

7. Realistic Topography

An important capability of the Green function method compared to previous analytic techniques used to study internal tide scattering is that it provides a relatively straightforward means for investigating realistic oceanic scenarios; this has been demonstrated for internal tide generation by *Echeverri and Peacock* [2010], albeit in the limit of the WKB approximation that has now been shown to potentially give misleading results. In this section, we use the complete Green function method to consider the role of the Line Islands Ridge in the scattering of the mode-1 internal tide radiated south-west from the Hawaiian Ridge, and we also study scattering of the mode-1 internal tide radiated north-east from the Hawaiian Ridge by small-scale, rough topography. These case studies use Smith-Sandwell topography data (http://www.nodc.noaa.gov/OC5/WOA05/pr_woa05.html) and representative stratification data obtained from the World Ocean Atlas (http://www.nodc.noaa.gov/OC5/WOA05/pr_woa05.html). The investigations assume 2-D internal tide dynamics along transects, which is of course an idealization of the real 3-D physical system. In support of the 2-D approach, *Johnston et al*. [2003] comment that the section of the Line Islands Ridge we consider, known as the Sculpin Ridge, is long and narrow and it would therefore seem conducive to a 2-D approximation. Overall, we would expect 2-D scattering to be more efficient than 3-D scattering, so the results obtained can be considered as providing an upper bound for the scattering efficiency. In several cases, direct comparisons are made with the results of 2-D numerical simulations to demonstrate the accuracy of the theoretical approach.

7.1. South of Hawaii

The Line Islands Ridge is a substantial topographic feature on the ocean floor located approximately 1000 km south-west of the Hawaiian Islands chain. A contour plot of a roughly 5° longitude by 5.5° latitude section of this ridge system, centered near 167.5°W and 15°N, is presented in Figure 11a. Satellite altimetry data reveal that a strong, semidiurnal mode-1 internal tide, generated at French Frigate Shoals in the Hawaiian Ridge, is incident from the north-east upon this section of the Line Islands Ridge [*Ray and Cartwright*, 2001]. Analysis of this altimetry data, supported by numerical simulation, suggests that in the vicinity of this location there is significant conversion from mode 1 to higher modes, accompanied by a rapid decay of mode-1 baroclinic energy flux [*Ray and Mitchum*, 1997; *Ray and Cartwright*, 2001; *Johnston et al*., 2003]. The opinion of *Johnston et al*. [2003] is that this is most likely a consequence of linear scattering by seafloor topography.

Figure 11b presents a typical stratification for the vicinity of the Line Islands Ridge, comprising a strong pycnocline in the upper few hundred meters and an exponential tail in the deep ocean. For this stratification, and using $\omega = 1.4053 \times 10^{-4}$ rad/s (M2) and $f = 3.76 \times 10^{-5}$ rad/s (corresponding to a latitude of 15°N), the mode-1 horizontal wavelength and phase speed are 1.45×10^5 m and 3.25 m/s, respectively, and the mode-2 horizontal wavelength and phase speed are 8.1×10^4 m and 1.81 m/s, respectively (assuming

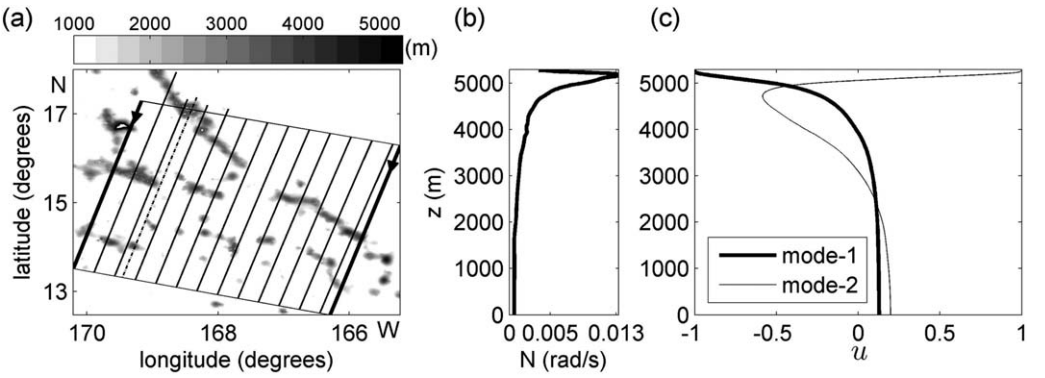

Figure 11. (a) A contour plot of the topography of the Line Islands Ridge, centered around 167.5°W and 15°N. The scattering of a mode-1 internal tide (incident in the direction of the black arrows) is investigated for 100 transects equispaced between the thick black lines. The scattered wavefield along the dashed line is presented in Figure 12. (b) A typical stratification for the vicinity of the Line Islands Ridge. (c) The vertical structure of horizontal velocity for modes 1 and 2 for the stratification presented in Figure 11b, with $\omega = 1.4053 \times 10^{-4}$ rad/s (M2) and $f = 3.76 \times 10^{-5}$ rad/s (15°N).

$H = 5300$ m). Plots of the vertical structure of the horizontal velocity for mode 1 and mode 2 are presented in Figure 11c.

We consider 100 different two-dimensional topographic cross sections within the domain shown in Figure 11a; this domain and the incident direction of the mode-1 internal tide match the scenario studied by *Johnston et al*. [2003]. Topography reaches within 1000–1500 m of the ocean surface in some locations, and outside this domain topography is assumed to smoothly descend to a constant ocean depth of 5300 m below the ocean surface over a distance of 26 km, as assumed by *Johnston et al*. [2003]. Exceptions to this are the black cross-sectional lines that protrude outside the box in Figure 11a for which the topography was instead interpolated from real data till the height reached 5300 m below the ocean surface. Within the domain, any topography that lies >5300 m below the ocean surface is set to $z = 0$, as the analysis requires $z \geq 0$ everywhere in the domain.

Figure 12 presents a snapshot of theoretical and numerical results for the incident-plus-scattered wavefields resulting from a mode-1 internal tide propagating along the dashed-line transect in Figure 11a. This transect contains a strongly supercritical ($\epsilon \approx 4.4$) feature near $x = -2 \times 10^5$ m, where the height ratio reaches values around $h^* = 0.69$. There is remarkably good qualitative agreement in the structure of the wavefields calculated by theory and numerics, both displaying the same sharp wave beams that suggest significant alteration of the incident mode-1 wavefield. The quantitative agreement for this transect and other sample transects is very good too, as summarized in Table 1.

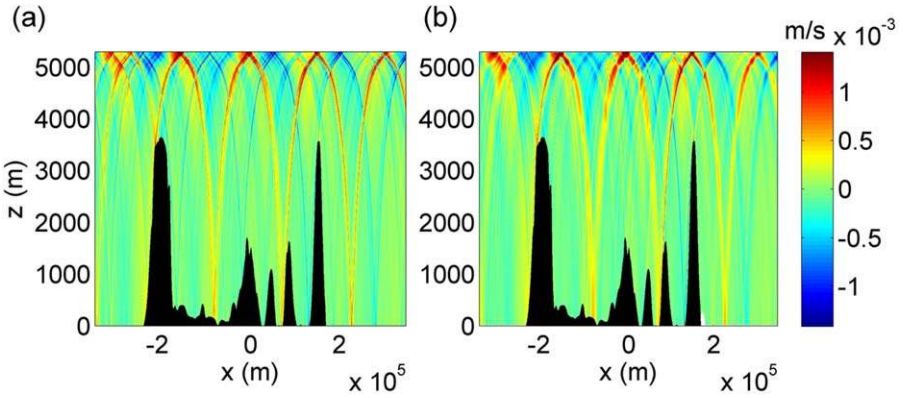

Figure 12. The horizontal velocity field $u(x,z,t)$ at an arbitrary instant in time for mode-1 (incident from the left) scattering along the dashed-line transect shown in Figure 11a. (a) Theoretical results and (b) numerical results.

Table 1. Comparison of Results From Analysis and Numerical Simulations for Four Different Transects Across the Line Islands Ridge Shown in Figure 11a[a]

	20		43		69		82	
Index	Theory	Numerics	Theory	Numerics	Theory	Numerics	Theory	Numerics
C_1^T	0.30	0.28	0.17	0.17	0.54	0.55	0.77	0.77
C_2^T	0.19	0.18	0.02	0.01	0.10	0.09	0.03	0.03
C_1^R	0.15	0.17	0.002	0.00025	0.01	0.007	0.005	0.006
C_2^R	0.06	0.06	0.32	0.31	0.12	0.10	0.02	0.02

[a]Index 20 is the dashed-line transect in Figure 11a.

A summary of the results for the different transects is presented in Figure 13, in which the scattering efficiency $C_{2-\infty}^{T+R}$ for every cross section is plotted as a colormap. Theory predicts that across all 100 transects, on average 76.5% of the incident mode-1 energy is transmitted and the remaining 23.5% is reflected. The topography along some of the transects is very efficient at scattering, with $C_{2-\infty}^{T+R}$ exceeding 80% in some cases, and on average $C_{2-\infty}^{T+R}$ is 40%, suggesting that scattering by the topography in this region is substantial. We recall that, of course, this is a 2-D analysis of a 3-D system and that isolated transects with localized, sharp peaks that lead to high scattering rates are likely to scatter less substantially in 3-D. The scattering efficiency varies quite smoothly across transects, however, suggesting a reasonably 2-D scenario, and even ignoring the most substantial peaks in the scattering efficiency the average value over all 100 cross sections is still 39%. These results compare favorably with the 3-D numerical results of *Johnston et al.* [2003]. In the same subdomain of the Line Islands Ridge region, they reported that 37% of the incident mode-1 energy flux is lost by scattering into modes 2–5 (19%), dissipation by turbulence (15%) and nonlinear transfer to the M_4 internal tide; we find around 40% of the incident energy is scattered into higher modes, with 24–28% of the energy going into modes 2–5.

7.2. North of Hawaii

We now proceed to consider a semidiurnal, mode-1 internal tide propagating north from Hawaii over realistic small-scale rough topography. Although the latitude is varying the model requires constant background rotation, which we choose to be $f = 8.34 \times 10^{-5}$ rad/s (corresponding to a latitude of 35°N). Figure 14a presents a colormap of the topography in the region, with several of the transects along which we perform our study marked. Figure 14b presents a representative stratification from the region shown in Figure 14a, and the corresponding mode-1 and mode-2 shapes for this stratification are presented in Figure 14c.

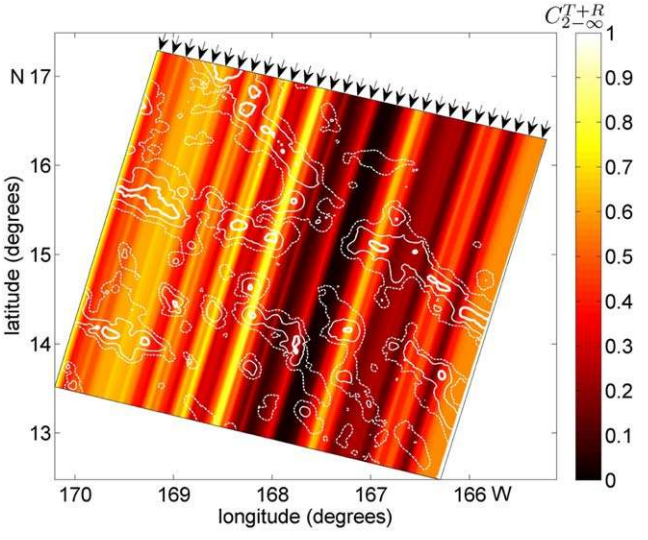

Figure 13. Summary of the scattering efficiency, calculated using the Green function model, for the 100 transects considered in the region of the Line Islands Ridge. The colormap represents the value of $C_{2-\infty}^{T+R}$ for each transect. The background contours are the isobaths 5000 m (dashed line), 4000 m (thin line), and 2000 m (thick line) below the ocean surface.

For our case studies, sections of differing length from every transect in Figure 14a are considered such that the ocean depth is at least 5250 m at the start and end points of every section, ensuring negligible scattering by the features at each end of every section. The total water depth for every section H is chosen to be 6000 m, and the topographic heights at the two ends of every section are smoothly extrapolated to $z = 0$. All topography that extends below $z = 0$ in any transect (i.e., deeper than 6000 m) is reset to have zero topographic height. Statistical analysis of the topography in the region reveals that the height ratio follows a Gaussian-like distribution about a mean value of $h^* = 0.053$. On average, topography is far from the pycnocline and is in the strongly

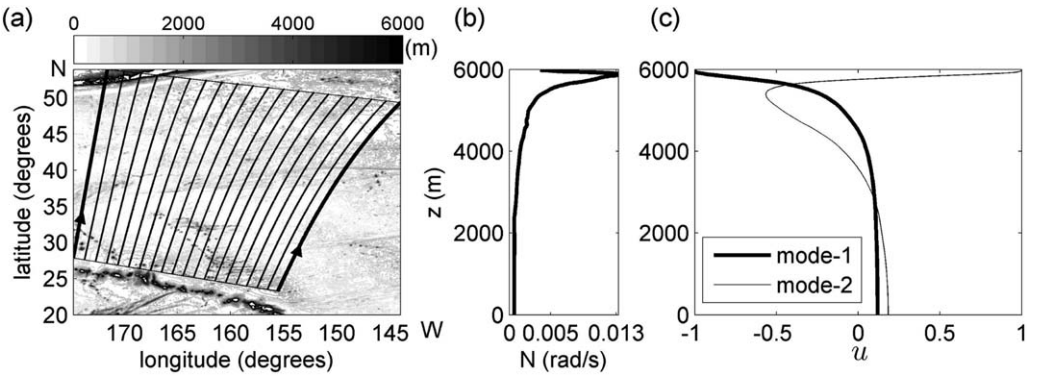

Figure 14. (a) A contour plot of the topography at the Hawaiian Ridge and northward regions over which we consider the propagation of the mode-1 internal tide (the heights are measured from a reference location that is 6000 m below the sea surface). Investigations are performed for 191 transects equispaced between the thick black lines (every 10th transect is shown), with the black arrows indicating the direction of propagation. (b) A typical stratification for the region shown in Figure 14a. (c) Horizontal velocity structure of modes 1 and 2 for the stratification presented in Figure 14b, with $\omega = 1.4053\times10^{-4}$ rad/s (M2) and $f = 8.34\times10^{-5}$ rad/s (35° N).

subcritical regime, although many transects contain at least one not-insignificant topographic feature with $h^* > 0.2$.

To quantify the scattering to higher modes for the region north of Hawaii, in Figure 15a, we plot $C_{T+R}^{2-\infty}$ for a mode-1 M_2 internal tide for 1500 km long sections of each of the 191 transects; the results from 2-D numerical simulations for 19 of these transects are also presented to provide further validation of the theoretical method. The average scattering efficiency is found to be a modest 8.8%. The length of sections of the transects used was then increased from 1000 to 3000 km in steps of 250 km, and the variation of average scattering efficiency, $\bar{C}_{T+R}^{2-\infty}$ with transect length is plotted in Figure 15b. Performing a linear fit of $\bar{C}_{T+R}^{2-\infty}$ as a function of the transect length, L_t, we obtain the relation $\bar{C}_{T+R}^{2-\infty} = 8.71\times10^{-8}\,L_t - 0.046$, the error bar for every value of L_t being computed using the standard deviation of $C_{T+R}^{2-\infty}$ over all the transects considered. When only those sections with $h^*_{max} < 0.4$ and $h^*_{max} < 0.2$ are considered, the slopes of the linear fit for $\bar{C}_{T+R}^{2-\infty}$ as a function of L_t decrease to 3.4×10^{-8} m^{-1} and 1.85×10^{-8} m^{-1}, respectively, suggesting that sections with larger values of h^*_{max} contribute significantly to the mean scattering efficiency. The slopes of the three straight lines can be interpreted as an increase in the scattering efficiency by 8.71%, 3.4%, and 1.85% for every 1000 km of topography.

The aforementioned results reveal that for transects of length 1000–3000 km with only small amplitude topography the efficiency of internal tide scattering is indeed an order 5–10% process. There is, however, an interesting caveat to these results that is suggested by data presented in Figure 15b and clarified by the results presented in Figure 16, in which $C_{T+R}^{2-\infty}$ is plotted as a function of the maximum height ratio, h^*_{max}, along each transect of length $L_t = 1.5\times10^6$ m (circles) and $L_t = 2.5\times10^6$ m (asterisks). There is a strong

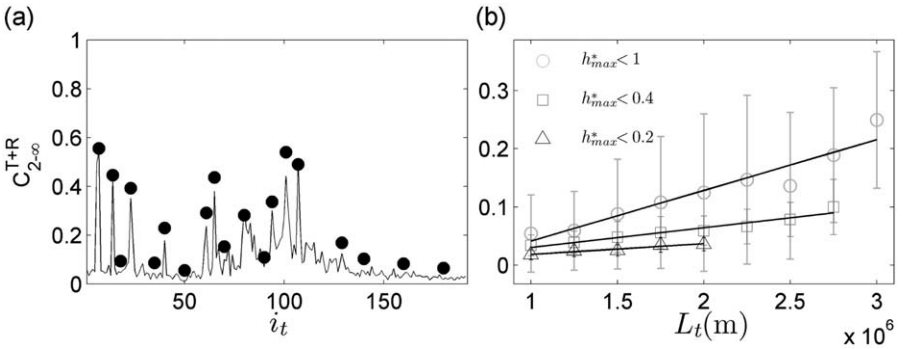

Figure 15. (a) The scattering efficiency $C_{2-\infty}^{T+R}$ for the 191 cross sections considered in Figure 14a for $L_t = 1.5\times10^6$m; the solid line presents results calculated using the Green function model and the black dots correspond to results from numerical simulations. The index i_t (1–191) denotes the transect number. (b) Average scattering efficiency, $\bar{C}_{2-\infty}^{T+R}$ as a function of L_t for sections with $h^*_{max} < 1$ (circles), $h^*_{max} < 0.4$ (squares), and $h^*_{max} < 0.2$ (triangles).

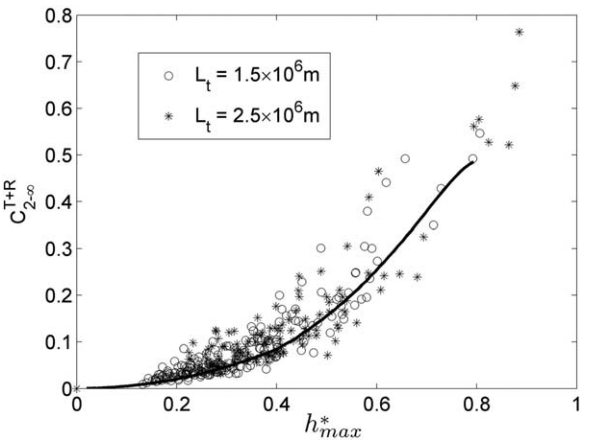

Figure 16. $C^{T+R}_{2-\infty}$ (calculated using the Green function model) as a function of the maximum height ratio h^*_{max} for transects with $L_t = 1.5\times10^6$ m (circles) and $L_t = 2.5\times10^6$ m (asterisks). The solid curve corresponds to $C^{T+R}_{2-\infty}$ for an isolated knife-edge topography of height ratio h^*_{max} in the stratification shown in Figure 14b.

correlation between the scattering efficiency along a transect and h^*_{max}. Indeed, for $h^*_{max} > 0.5$ the scattering efficiency readily exceeds 20% and for $h^*_{max} > 0.65$ the scattering efficiency approaches 40%, which corresponds to the case of the Line Islands ridge. For comparison, superimposed on the data is the scattering efficiency of an isolated knife-edge topography as a function of height ratio for the same stratification. From the close fit of the theoretical curve to the predictions based on real ocean topography, it is evident that the scattering efficiency for a transect is dominated by the scattering due to the tallest topographic feature along that transect. Again, we remind ourselves that this is a 2-D study and introducing three-dimensionality will likely reduce these values, but if internal tide generation results are anything to go by then these findings are not unreasonable provided the length of the topographic feature obstructing the internal tide is at least three times the width of the ridge in the direction of propagation of the internal tide [*Holloway and Merrifield*, 1999].

8. Conclusions

In this paper, the recently advanced Green function method that accounts for fully nonuniform stratifications without the WKB approximation has been used to investigate scattering of the mode-1 internal tide by ocean-floor topography. This robust semianalytical technique, which works for any arbitrarily shaped two-dimensional topographies (with both the end points at the ocean bottom $z = 0$) in arbitrary stratifications, enabled systematic investigation of a wide range of idealized and realistic scenarios. In all cases, the results of the analysis were validated by direct comparisons with the results of numerical simulations. Furthermore, it was shown that the results from the WKB approach can be misleading even for modest sized ridges.

For isolated Gaussian topography in both uniform and nonuniform stratifications, the transmission and reflection of energy flux, and the efficiency of scattering out of mode 1 both depend on the criticality and the depth ratio. The results for a nonuniform stratification typical of the ocean are qualitatively the same as those for a constant stratification, albeit with the key features shifted to larger height ratios, but there are significant discrepancies between the predictions of the complete Green function theory and approximate WKB results, revealing that the latter are not appropriate for reliable ocean predictions. Two key results are that large amplitude critical topography is the most efficient at mode-1 scattering and small amplitude topography scatters with an efficiency on the order of 5–10% for transects of length 1000–3000 km.

The methods developed in this paper were directly applied to the geophysical setting of the Hawaiian Ridge, representing the first attempt to quantify scattering by realistic ocean topography in a realistic stratification. To the south, the Line Islands ridge has been shown to be efficient at converting a significant fraction of the incident mode-1 energy flux to higher modes. To the north, we find that any realistic, small-amplitude, rough topography scatters around 5–10% of the energy out of mode 1 for distances in the range 1000–3000 km, this value increasing systematically but fairly modestly with the propagation distance. Significantly, however, there is a very strong correlation between the scattering efficiency along a transect and the maximum topographic height along a transect, revealing that one large topographic feature along the path of the internal tide can be primarily responsible for scattering. Therefore, a reasonable approach for making an estimate of scattering along a transect is to find the tallest supercritical topographic feature in the transect, replace it with a knife edge of the same height and calculate the scattering efficiency of this

equivalent isolated knife-edge topography. If there is no standout large topographic feature the full analysis must be performed for that particular transect.

Given that any internal tide is likely to encounter at least one tall feature along its path, we conclude that scattering by ocean floor topography can be a significant mechanism to transfer energy from large to small spatial scales. At such locations, due to the scattering of the low-mode internal tide to higher modes, one might expect to find a mixing hot spot. These results are based on the assumption of two-dimensional topography, however, and should be considered an upper bound for the scattering efficiency. While recent studies [*Legg* 2014] suggest that scattering of low-mode internal tides normally incident on a 3-D, convex slope is similar to the 2-D infinite ridge scenario, further studies are needed to properly assess the efficiency of scattering by large-scale, three-dimensional topography. Furthermore, it would be a useful exercise to determine how typical it is for a low-mode internal tide originating from a deep-ocean generation site to encounter a large seamount or ridge before reaching the continental shelf. Finally, laboratory experiments to investigate the nonlinear regimes of scattering that the complete Green function approach cannot model could provide key insights, as seen in the preliminary experiments of *Peacock et al.* [2009].

Acknowledgments

T.P. acknowledges funding from National Science Foundation grants OCE 0645529 and OCE1129757. G.S.C. acknowledges funding from the National Science Foundation grant OCE 0825266. The authors acknowledge Neil Balmforth for suggesting the form of Figure 16. Request for access to the data presented in this paper can be sent to manims@ae.iitm.ac.in.

References

Balmforth, N. J., and T. Peacock (2009), Tidal conversion by supercritical topography, *J. Phys. Oceanogr.*, *39*, 1965–1974.

Blumberg, A. F., and G. L. Mellor (1987), A description of a three-dimensional coastal ocean circulation model, in *Three-Dimensional Coastal Ocean Models, Coastal Estuarine Sci.*, vol. 4, edited by N. S. Heaps, pp. 1–16, AGU, Washington, D. C.

Bühler, O., and M. Holmes-Cerfon (2011), Decay of an internal tide due to random topography in the ocean, *J. Fluid Mech.*, *678*, 271–293.

Carter, G. S., and M. A. Merrifield (2007), Open boundary conditions for regional tidal simulations, *Ocean Modell.*, *18*, 194–209.

Carter, G. S., M. A. Merrifield, J. M. Becker, K. Katsumata, M. C. Gregg, D. S. Luther, M. D. Levine, T. J. Boyd, and Y. L. Firing (2008), Energetics of M_2 barotropic-to-baroclinic tidal conversion at the Hawaiian islands, *J. Phys. Oceanogr.*, *38*, 2205–2223.

Cox, C. S., and H. Sandstrom (1962), Coupling of internal and surface waves in water of variable depth, *J. Oceanogr. Soc. Jpn.*, *20*, 499–513.

Echeverri, P., and T. Peacock (2010), Internal tide generation by arbitrary two-dimensional topography, *J. Fluid Mech.*, *659*, 247–266.

Echeverri, P., M. R. Flynn, K. B. Winters, and T. Peacock (2009), Low-mode internal tide generation by topography: An experimental and numerical investigation, *J. Fluid Mech.*, *636*, 91–108.

Egbert, G. D., and R. D. Ray (2000), Significant dissipation of tidal energy in the deep ocean inferred from satellite altimeter data, *Nature*, *405*, 775–778.

Garrett, C., and E. Kunze (2007), Internal tide generation in the deep ocean, *Annu. Rev. Fluid Mech.*, *39*, 57–87.

Gilbert, D., and C. Garrett (1989), Implications for ocean mixing of internal wave scattering off irregular topography, *J. Phys. Oceanogr.*, *19*, 1716–1729.

Holloway, P. E., and M. A. Merrifield (1999), Internal tide generation by seamounts, ridges, and islands, *J. Geophys. Res.*, *104*(C11), 25,937–25,951.

Johnston, T. M. S., and M. A. Merrifield (2003), Internal tide scattering at seamounts, ridges and islands, *J. Geophys. Res.*, *108*(C6), 3180, doi: 10.1029/2002JC001528.

Johnston, T. M. S., M. A. Merrifield, and P. E. Holloway (2003), Internal tide scattering at the line islands ridge, *J. Geophys. Res.*, *108*(C11), 3365, doi:10.1029/2003JC001844.

Kunze, E., and S. G. Llewellyn Smith (2004), The role of small-scale topography in turbulent mixing of the global ocean, *Oceanography*, *17*, 55–64.

Larsen, L. H. (1969), Internal waves incident upon a knife edge barrier, *Deep Sea Res. Oceanogr. Abstr.*, *16*, 411–419.

Legg, S. (2014), Scattering of low-mode internal waves at finite isolated topography, *J. Phys. Oceanogr.*, *44*, 359–383.

Llewellyn Smith, S. G., and W. R. Young (2002), Conversion of the barotropic tide, *J. Phys. Ocean.*, *32*, 1554–1556.

Llewellyn Smith, S. G., and W. R. Young (2003), Tidal conversion at a very steep ridge, *J. Fluid Mech.*, *495*, 175–191.

MacKinnon, J. A., and K. B. Winters (2005), Subtropical catastrophe: Significant loss of low-mode tidal energy at 28.9°, *Geophys. Res. Lett.*, *32*, L15605, doi:10.1029/2005GL023376.

Mathur, M., and T. Peacock (2009), Internal wave beam propagation in nonuniform stratifications, *J. Fluid Mech.*, *639*, 133–152.

Mathur, M., and T. Peacock (2010), Internal wave interferometry, *Phys. Rev. Lett.*, *104*, 118501.

Müller, P., and X. Liu (2000a), Scattering of internal waves at finite topography in two dimensions. Part I: Theory and case studies, *J. Phys. Oceanogr.*, *30*, 532–549.

Müller, P., and X. Liu (2000b), Scattering of internal waves at finite topography in two dimensions. Part II: Spectral calculations and boundary mixing, *J. Phys. Oceanogr.*, *30*, 550–563.

Müller, P., and N. Xu (1992), Scattering of oceanic internal gravity waves off random bottom topography, *J. Phys. Oceanogr.*, *22*, 474–488.

Munk, W., and C. Wunsch (1998), Abyssal recipes II: Energetics of tidal and wind mixing, *Deep Sea Res., Part I*, *45*, 1977–2010.

New, A. L., and J. C. B. Da Silva (2002), Remote sensing evidence for the local generation of internal soliton packets in the central Bay of Biscay, *Deep Sea Res., Part I*, *49*, 915–934.

New, A. L., and R. D. Pingree (1992), Locan generation of internal soliton packets in the central bay of Biscay, *Deep Sea Res., Part A*, *39*, 1521–1534.

Peacock, T., M. J. Mercier, H. Didelle, S. Viboud, and T. Dauxois (2009), A laboratory study of low-mode internal tide scattering by finite-amplitude topography, *Phys. Fluids*, *21*, 121702.

Pétrélis, F., S. G. Llewellyn Smith, and W. R. Young (2006), Tidal conversion at a submarine ridge, *J. Phys. Oceanogr.*, *36*, 1053–1071.

Rainville, L., and R. Pinkel (2006), Propagation of low-mode internal waves through the ocean, *J. Phys. Oceanogr.*, *36*, 1220–1236.

Ray, R. D., and D. E. Cartwright (2001), Estimates of internal tide energy fluxes from Topex/Poseidon altimetry: Central North Pacific, *Geophys. Res. Lett.*, *28*(7), 1259–1262.

Ray, R. D., and G. T. Mitchum (1997), Surface manifestation of internal tides in the deep ocean: Observations from altimetry and island gauges, *Prog. Oceanogr.*, *40*, 135–162.

Robinson, R. M. (1969), The effects of a barrier on internal waves, *Deep Sea Res. Oceanogr. Abstr.*, *16*, 421–429.
Rubenstein, D. (1988), Scattering of inertial waves by rough bathymetry, *J. Phys. Oceanogr.*, *18*, 5–18.
Rudnick, D. L., et al. (2003), From tides to mixing along the Hawaiian ridge, *Science*, *301*, 355–357.
St. Laurent, L. C., and C. Garrett (2002), The role of internal tides in mixing the deep ocean, *J. Phys. Oceanogr.*, *32*, 2882–2899.
Staquet, C., and J. Sommeria (2002), Internal gravity waves: From instabilities to turbulence, *Annu. Rev. Fluid Mech.*, *34*, 559–593.
Sutherland, B. R., and K. Yewchuk (2004), Internal wave tunnelling, *J. Fluid Mech.*, *511*, 125–134.
Tsang, Y. K., W. R. Young, and N. J. Balmforth (2008), Near-inertial parametric subharmonic instability, *J. Fluid Mech.*, *607*, 25–49.
Zhao, Z., M. H. Alford, and J. B. Girton (2012), Mapping low-mode internal tides from multisatellite altimetry, *Oceanography*, *25*(2), 42–51.